Dominance of correlation and relativistic effects on photodetachment time delay well above threshold

Soumyajit Saha, Pranawa C. Deshmukh, Anatoli S. Kheifets, and Steven T. Manson

Phys. Rev. A **99**, 063413 — Published 17 June 2019

DOI: 10.1103/PhysRevA.99.063413

Dominance of correlation and relativistic effects on photodetachment time delay well above threshold

Soumyajit Saha,[1,*] Pranawa C. Deshmukh,[2,3,†] Anatoli S. Kheifets,[4,‡] and Steven T. Manson[5,§]

[1] *Department of Physics, Indian Institute of Technology Madras, Chennai 600036, India*
[2] *Department of Physics, Indian Institute of Technology Tirupati, Tirupati, 517506, India*
[3] *Department of Physics, Indian Institute of Science Education and Research Tirupati, Tirupati, 517507, India*
[4] *Research School of Physics and Engineering, The Australian National University, Canberra ACT 2601, Australia*
[5] *Department of Physics and Astronomy, Georgia State University, Atlanta, 30303, USA*

(Dated: May 15, 2019)

Wigner time delay in photodetachment from the $3p_{3/2}$ and $3p_{1/2}$ subshells of Cl^- have been studied in the vicinity of the $2p_{3/2}$ and $2p_{1/2}$ thresholds, using the relativistic random phase approximation (RRPA). The results show time delay spectra dominated by many-body correlations along with very complicated dependence on the energy over a broad spectral range. In addition, the time delay spectra of the two spin-orbit split $3p$ subshells differ significantly from one another, thereby revealing the importance of relativistic effects even in the case of a low-Z system.

PACS numbers: 32.80.Rm 32.80.Fb 42.50.Hz

I. INTRODUCTION

Probing Wigner time delay [1–3] in photoemission unearths the motion of electrons in transition in the real time domain, i.e., at the attosecond level. Modern studies of photoemission time delay have been triggered by pioneering experiments on the Ne [4] and Ar [5] atoms that opened a new avenue to explore the ultrafast electron dynamics of atomic and molecular (and condensed matter) systems, and led to a plethora of recent theoretical and experimental studies of time delay over a broad range of systems. Much of this work is reviewed in [6], and [7–24] provide a representative selection of more recent investigations. Aside from the interest in time delay as an indicator of electron transition dynamics on the attosecond time scale, since the time delay is related to the energy derivative of the phase of the transition matrix element [1–3], it also provides information on the most elusive part of it, the phase; the magnitude can be obtained much more easily from the respective cross sections.

In general, it had been seen that, in almost all the cases, the time delay for the photoionization of a given atomic or molecular subshell approaches zero with increasing photoelectron kinetic energy [6–8]. However, it is known that outer-shell photoionization is affected by correlation in the vicinity of inner-shell thresholds; this aspect of correlation is known as interchannel coupling and its effects have been seen in photoionization cross sections and angular distributions both theoretically and experimentally; see [25] and references therein. Very recently, it was shown that these interchannel coupling effects extend to time delay significantly as well [21]. Specifically, it was shown that, over a broad range of atoms and energies, the Wigner time delay for outer-shell photoemission that was effectively zero below an inner-shell threshold, experiences a significant jump above the inner-shell threshold, as much as about 30 as. Above the inner threshold, however, the magnitude of time delay was found to decrease monotonically.

These investigations have prompted us to look at time delay in negative ions whose photoemission is known to be dominated by correlation [26]; also very little is known about photodetachment time delay [27, 28]. In addition, time delay is generally measured using two photons, so that the total time delay, $\tau = \tau_w + \tau_{cc}$, where, τ_w is the Wigner time delay and τ_{cc} is continuum-continuum (Coulomb-laser-coupling) correction, a measurement-induced delay due to the electron being probed by the second (laser) photon in a long-range potential with a Coulomb tail of charge Z [27, 29]. Of importance here is that τ_{cc} effectively vanishes when the atomic potential is short-range, as in photodetachment, making the interpretation of experiment much more straightforward [27]. Ar-like Cl^- has been chosen for this study, and we look at $3p$ photodetachment in the vicinity of the $2p$ thresholds; among the reasons for this choice are the closed-shell nature of the ion that facilitates interpretation of the results, and that there are inner shells in an experimentally-convenient region. The results demonstrate: that the interchannel effects on time delay in negative ions are far greater than in neutral atoms; that the energy dependence is far more complex than the simple decreasing behavior of atoms; that relativistic effects play a vital role, even at such low Z; and that these effects extend over tens of eV.

The theoretical method has been presented in Sec. II. In Sec, III, we present and discuss our results. Conclusions are drawn in section IV.

*Electronic address: soumyajit147@gmail.com
†Electronic address: pcd@iittp.ac.in
‡Electronic address: a.kheifets@anu.edu.au
§Electronic address: smanson@gsu.edu

TABLE I: Theoretical and experimental [33] photodetachment thresholds of Cl^- in eV.

Subshell(Cl^-)	DF(eV)	Exp.(eV)	Subshell(Cl^-)	DF(eV)
$3p_{3/2}$	4.03	3.62	$3s_{1/2}$	20.13
$3p_{1/2}$	4.17	3.73	$2p_{3/2}$	208.87
			$2p_{1/2}$	210.64
			$2s_{1/2}$	280.22

II. THEORETICAL METHOD

A relativistic formulation is required to investigate effects due to spin-orbit-splitting of the $2p$ thresholds, and to study the time delay in both the $3p_{3/2}$ and $3p_{1/2}$ subshells individually. The relativistic random phase approximation (RRPA) [30], based on the Dirac equation, and which includes both initial-state and final-state correlation, is employed for the present calculations, along with our previously-reported theoretical development [15]. Specifically, in the RRPA methodology, the initial state can be characterized by a large configuration interaction (CI) wave function including the single-particle initial state of Dirac-Fock (DF) orbitals, plus all two-identical-particle two-identical-hole excitations, also of DF orbitals, summed to infinity, e.g., for the outer $3p^6$ of Cl^- added are all of the $3p^4nl^2$ configurations, etc. This represents a highly-correlated initial state wave function. The final continuum state can also be characterized as a CI wave function in which all of the single excitation wave functions are mixed; for continuum wave functions this is known as interchannel coupling. Of importance that both continuum (ionization) and discrete wave functions are included, meaning that core-excited Fano resonances are implicitly included. Aside from being relativistic *ab initio*, RRPA is gauge-invariant, and it allows the possibility of performing truncated calculations in which certain channels are omitted as a means of pinpointing the specific interchannel coupling responsible for various observable effects. We consider incident photons linearly polarized in the z-direction, and we investigate the time delay, which is angle-dependent in general [23, 31, 32], in the direction parallel to the polarization.

The five possible relativistic transitions from $3p$ subshell are $3p_{1/2} \rightarrow \varepsilon s_{1/2}, \varepsilon d_{3/2}$ and $3p_{3/2} \rightarrow \varepsilon s_{1/2}, \varepsilon d_{3/2}, \varepsilon d_{5/2}$. For a transition from an initial state, $a(ljm)$, to the symmetry allowed final states, $\bar{a}(\bar{l}\bar{j}\bar{m})$, we define the dipole matrix element [15]

$$D_{n\kappa\rightarrow E\bar{\kappa}} = i^{1-\bar{l}} e^{i\delta_{\bar{\kappa}}} \left\langle \bar{a} \| Q_1^{(1)} \| a \right\rangle \ , \tag{1}$$

where,

$$\left\langle \bar{a} \| Q_1^{(1)} \| a \right\rangle = (-1)^{j+1/2} [\bar{j}][j] \begin{pmatrix} j & \bar{j} & J \\ -1/2 & 1/2 & 0 \end{pmatrix} \pi(\bar{l}, l, J-\lambda+1) R^{(1)}(\bar{a}, a) \tag{2}$$

is the (complex) reduced matrix element for an electric dipole transition and $\delta_{\bar{\kappa}}$ is the phase of the continuum wave with $\bar{\kappa} = \mp(\bar{j} + \frac{1}{2})$ for $\bar{j} = (\bar{l} \pm \frac{1}{2})$, The axially symmetric transition amplitudes contributing to the photodetachment process in the polarization z direction are:

$$\begin{aligned} T_{3p_{1/2}} &= +\frac{1}{\sqrt{6}} Y_{00} D_{3p_{1/2}\rightarrow\varepsilon s_{1/2}} + \frac{1}{\sqrt{15}} Y_{20} D_{3p_{1/2}\rightarrow\varepsilon d_{3/2}} \\ T_{3p_{3/2}} &= +\frac{1}{\sqrt{6}} Y_{00} D_{3p_{3/2}\rightarrow\varepsilon s_{1/2}} - \frac{1}{5\sqrt{6}} Y_{20} D_{3p_{3/2}\rightarrow\varepsilon d_{3/2}} \\ &\quad -\frac{1}{5}\sqrt{\frac{3}{2}} Y_{20} D_{3p_{3/2}\rightarrow\varepsilon d_{5/2}}. \end{aligned} \tag{3}$$

Here Y_{lm} are the spherical harmonics evaluated in the direction of polarization, and all of the phase information is contained in the $D's$. Note that the angular momentum algebra is the same in a single-particle framework and for a closed-shell atomic system, so that the resulting formulae are identical except for one crucial difference. The radial matrix element $R^{(1)}(\bar{a}, a)$ is obtained including all of the correlations (discussed above) in the RRPA calculation, i.e., the many-body effects included in RRPA are contained in the radial matrix elements. The Wigner time delay, in atomic units $e = \hbar = m = 1$, is simply the energy derivative of the phase of the ampli-

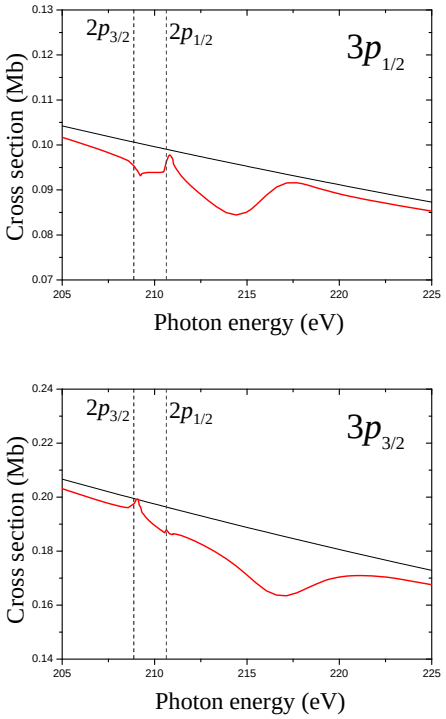

FIG. 1: (color online) Photodetachment cross sections for the $3p_{1/2}$ subshell of Cl^- (upper panel) and the $3p_{3/2}$ subshell (lower panel) in the vicinity of the $2p$ thresholds calculated at the 14-channel (thick red curve) and 7-channel (thin black curve) levels as explained in text. The $2p$ thresholds are indicated by vertical dashed lines.

tude,

$$\tau_{3p_j} = \frac{d}{dE} \tan^{-1} \left[\frac{\mathrm{Im} T_{3p_j}}{\mathrm{Re} T_{3p_j}} \right] \quad (4)$$

As mentioned earlier, final state correlations are included via interchannel coupling in truncated RRPA by performing the calculations coupling all the 14 relativistic dipole channels originating from the $3p$, $3s$, $2p$ and $2s$ subshells:

$$\begin{aligned} 3p_{3/2} &\rightarrow \varepsilon d_{5/2}, \varepsilon d_{3/2}, \varepsilon s_{1/2}; \\ 3p_{1/2} &\rightarrow \varepsilon d_{3/2}, \varepsilon s_{1/2}; \\ 3s_{1/2} &\rightarrow \varepsilon p_{3/2}, \varepsilon p_{1/2}; \end{aligned}$$

$$\begin{aligned} 2p_{3/2} &\rightarrow \varepsilon d_{5/2}, \varepsilon d_{3/2}, \varepsilon s_{1/2}; \\ 2p_{1/2} &\rightarrow \varepsilon d_{3/2}, \varepsilon s_{1/2}; \\ 2s_{1/2} &\rightarrow \varepsilon p_{3/2}, \varepsilon p_{1/2}. \end{aligned}$$

The $1s$ channels are omitted since the $1s$ threshold is so far away energetically (about 3 keV) that these channels have negligible effect on photoemission in the 210 eV vicinity of the $2p$ thresholds. To emphasize the effects of the inner-shell channels, calculations have been also performed coupling only the seven $3p$ and $3s$ channels:

$$\begin{aligned} 3p_{3/2} &\rightarrow \varepsilon d_{5/2}, \varepsilon d_{3/2}, \varepsilon s_{1/2}; \\ 3p_{1/2} &\rightarrow \varepsilon d_{3/2}, \varepsilon s_{1/2}; \\ 3s_{1/2} &\rightarrow \varepsilon p_{3/2}, \varepsilon p_{1/2}. \end{aligned}$$

The RRPA uses Dirac-Fock (DF) photoemission threshold energies, given in Table 1 and compared with available experimental thresholds [33].

III. RESULTS AND DISCUSSION

The results for the cross sections for the two spin-orbit-split $3p$ channels are shown in Fig. 1. Of interest in these results is that there is significant structure in the fully coupled cross sections for both cases in the neighborhood of the $2p$ thresholds, while the 7-channel results are smooth and monotonically decreasing; it is, thus, evident that it is the interchannel coupling of the $3p$ photodetachment channels with the $2p$ that is responsible for the structure. To understand this phenomenology, the total and subshell cross sections are shown in Fig. 2, in the region of the $2p$ thresholds, where it is clear that the $2p$ cross sections are more than an order of magnitude larger than the $3p$ (note the logarithmic scale), so that interchannel coupling between the channels from $3p$ and $2p$ alters the $3p$ photodetachment strength considerably.

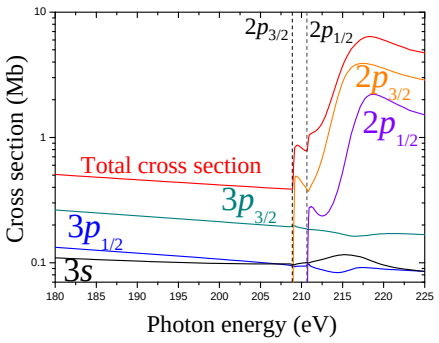

FIG. 2: (color online) Total photodetachment cross section and subshell cross sections calculated at the 14-channel level. The $2p$ thresholds are indicated by vertical dashed lines.

This phenomenon has been known for some time [25, 34]; what is new here is the complicated energy dependence of the perturbed cross sections, and that this is the first indication of the phenomenon in a negative ion. The structure in the $3p$ cross section mirrors the structure in the $2p$ cross sections, in a general sense. Very close to the $2p$ thresholds, the $3p$ cross sections acquire a structure that is characteristic of the $2p \rightarrow \varepsilon s$ channels, which dominate the $2p$ cross sections near threshold because the centrifugal barrier repels the photoelectron in the d-partial wave. Furthermore, several eV above threshold, the structure acquired by the $3p$ cross sections is characteristic of the $2p \rightarrow \varepsilon d$ shape resonances, produced by the centrifugal potential, which dominate the $2p$ cross sections in this region. Note that the correlated cross section is always below the uncorrelated one, indicating that the contribution of interchannel coupling is of the opposite sign from the unperturbed matrix elements. It is also evident, from Fig. 1, that the structures in the two cross sections are rather different, both between the two $2p$ thresholds, and above, e.g., the dip in the $3p_{1/2}$ cross section occurs at 214 eV, while the dip in the $3p_{3/2}$ cross section is seen at 217 eV. This is a clear indication of relativistic interactions, which is somewhat surprising at such a low Z. It is noteworthy that in the threshold region of Cl^- photodetachment, no relativistic effects were evident [35]. This indicates that the relativistic effects in the $3p$ photodetachment are intimately connected with the interchannel coupling with the $2p$ photoemission channels. Unfortunately, there are no existing experimental results for comparison, in this case, to assess the accuracy of these theoretical predictions. Note, however, that the same theoretical methodology yields excellent agreement with experiment for the isoelectronic Ar atom [31].

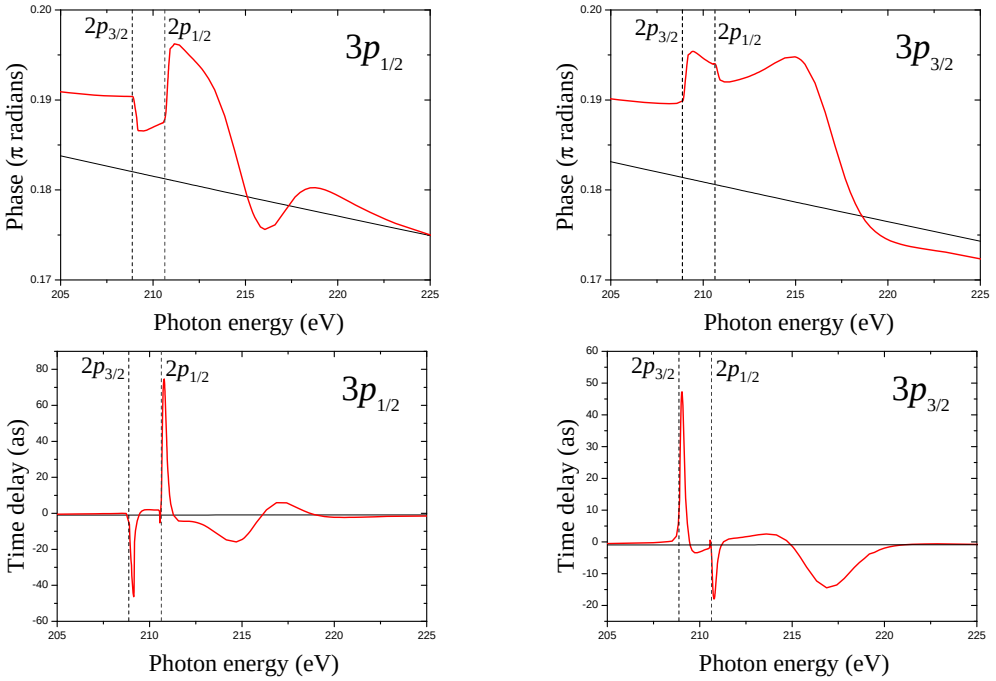

FIG. 3: (color online) Phases of the $3p_{1/2}$ subshell of Cl^- (upper left panel) and the $3p_{3/2}$ subshell (upper right panel) and time delays (lower left and lower right panels, respectively) in the vicinity of the $2p$ thresholds calculated at the 14-channel (thick red curve) and 7-channel (thin black curve) levels as explained in text. The $2p$ thresholds are indicated by vertical dashed lines.

Note also that the interesting structure is in the $2p$ photodetachement is exhibited at rather high photon energies, thus also high photoelectron kinetic energies. At these high energies, the long range effects of the Coulomb potential should be quite small. So why is photodetachment in this energy region still so different from photoionization? The answer lies with the nature of interchannel coupling. The cross section without the interchannel coupling included is structureless (see Fig. 1) and rather similar to the uncoupled result for the isoelectronic atom, Ar. However, with the interchannel coupling included, the $3p$ cross sections take on significant aspects of the character of the $2p$ cross sections. And these $2p$ cross sections are in their threshold region with low energy photoelectrons so that the Coulomb potential (or lack thereof) is a strong factor in the region near the $2p$ thresholds, even though this photon energy region produces rather high energy $3p$ photoelectrons. In other words, the differences in the near-threshold $2p$ cross sections between atom and ion are exactly what causes the difference. Clearly then, the structure in the $3p$ cross sections and time delays are manifestations of the structure in the $2p$ cross sections (Fig. 2).

In any case, it is clear that correlation in the form of interchannel coupling introduces significant structure in the magnitudes of the photoionization amplitudes. It is, thus, likely that the phases are similarly affected. This is exactly what happens, as seen in the upper panels of Fig. 3, where the 7-channel phases are monotonically decreasing, which is a characteristic of the unperturbed phases well above their thresholds, while the perturbed 14-channel phases exhibit considerably complicated structure. This behavior is a significant departure from the corresponding case in neutral atomic photoionization where the magnitude of the phase induced by interchannel coupling is maximal at the inner-shell threshold, then falls off monotonically with increasing energy [21]. As discussed in connection with the cross sections, very close to the $2p$ thresholds, the phase arises from the interchannel coupling with the $2p \rightarrow \varepsilon s$ channels, while at higher energies, the interaction with the $2p \rightarrow \varepsilon d$ channels, with their associated shape resonances, is the crucial perturbation. It is also noteworthy that the phases of the spin-orbit split $3p$ amplitudes obtained in the 14-channel result are seen to be markedly different from each other (Fig. 3), thus emphasizing that the phases too are strongly affected by relativistic interactions. Without the correlation induced by interchannel coupling, Fig. 3 shows that the two $3p$ phases are essentially the same.

The Wigner time delays generated from the phases, Eq. (4), are shown in the lower panels of Fig. 3 for the $3p_{1/2}$ and $3p_{3/2}$ subshells of Cl^-. The outstanding aspect of these results is a dramatic energy dependence of the time delay spectra, reaching large positive and large negative values over a relatively small energy range, along with the fact that relativistic effects cause the time delays in the two cases to be rather significantly different. The $3p_{1/2}$ time delay is seen to exhibit a large and negative

spike, just above the $2p_{3/2}$ threshold, while the $3p_{3/2}$ time delay shows a large and positive spike; and the reverse occurs just above the $2p_{1/2}$ threshold. This can be explained from the lowest order perturbation theory analysis [21] which equates the imaginary part of the inter-shell correlation-induced amplitude to the dipole matrix element of the transition in the inner shell, $2p_{1/2} \rightarrow \epsilon s_{1/2}$ and $2p_{3/2} \rightarrow \epsilon s_{1/2}$ in the present case. From Eq. (2) it can be seen that these matrix elements have opposite signs and differ by a factor of $\sqrt{2}$. At somewhat higher energies, both $3p_{1/2}$ and $3p_{3/2}$ time delays display indications of the interchannel coupling with the $2p \rightarrow \varepsilon d$ shape resonances, albeit the manifestation in the two cases is seen to be rather different. This is so because all the dipole matrix elements in the $2p_j \rightarrow \epsilon d_{\bar{j}}$ channels have the same sign. Note that the black lines in the lower two panels of Fig. 3 are the 7-channel (i.e., without coupling the $2p$ channels) $3p_{1/2}$ and $3p_{3/2}$ Wigner time delays, *not* the *y equals to* zero line. This demonstrates that all of the phenomenology exhibited in the $3p$ time delays is the result of correlation in the form of interchannel coupling. These results are in sharp contrast to photoionization of the neutral Ar atom (which is isoelectronic to Cl^-, where the time delays are monotonically decreasing in magnitude above the $2p$ thresholds, i.e., they are devoid of any structure. It is, thus, evident, that the effects of multielectron correlation, in the form of interchannel coupling, on the Wigner time delay of an outer-shell photoemission in the neighborhood of inner-shell thresholds for negative ion photodetachment differs markedly, both quantitatively and qualitatively, from photoemission from neutral atoms.

The separation of the $3p_{1/2}$ and $3p_{3/2}$ thresholds is only slightly more than 0.1 eV, so that the individual time delays might not be resolved in a particular experiment. Thus, the unresolved (average) $3p$ time delay has been calculated, the $3p_{1/2}$ and $3p_{3/2}$ time delay weighted by their respective cross sections, i.e.,

$$\tau_{3p} = \frac{\tau_{3p_{1/2}}|T_{3p_{1/2}}|^2 + \tau_{3p_{3/2}}|T_{3p_{3/2}}|^2}{|T_{3p_{1/2}}|^2 + |T_{3p_{3/2}}|^2} \qquad (5)$$

and the results are shown in Fig. 4. Although some of the physics of the individual subshell time delay is lost in the average, Fig. 4 shows very significant narrow structure immediately above each $2p$ threshold, owing to the $2p \rightarrow \varepsilon s$ transitions. The broader structures at somewhat higher energies are traced to the $2p \rightarrow \varepsilon d$ shape resonances. The 7-channel result, without the interchannel coupling, is seen to be essentially zero in Fig. 4. It is evident then, that, despite the averaging process inherent in examining only the unresolved time delay, there is still important physics remaining; consequently, this is a very attractive case for experimental investigation. Furthermore, there is nothing special about the case of Cl^- photodetachment. Cl^- was chosen as a test case because the similar situation in neutral Ar photoemission has been studied [21]. But the effective details in this report should be exhibited generally in the photodetachment time delay of outer shell in the vicinity of inner thresholds, although the details will vary both qualitatively and quantitatively, with each case.

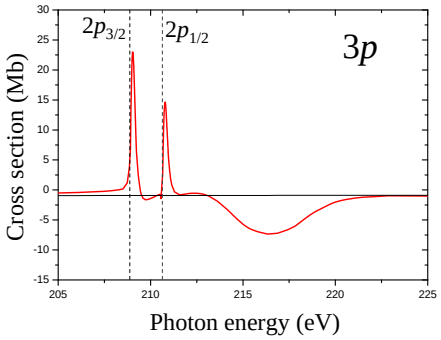

FIG. 4: Wigner time delay of the unresolved $3p$ subshell of Cl^- in the vicinity of the $2p$ thresholds calculated at the 14-channel (thick red curve) and 7-channel (thin black curve) levels as explained in text. The $2p$ thresholds are indicated by vertical dashed lines.

The two-photon XUV +IR RABBITT appears to be the most appropriate technique for time-delay measurements in negative ions. Although the target density will be low, the cross sections are still large enough so that the experiment should be doable, given the expected XUV intensity. In addition, the pulse trains available for RABBITT measurements have already reached the 100 eV photon energy mark [16, 36]. And, as the progress of attosecond science is very rapid, it won't be too long before 200 eV photon energy range becomes available for RABBITT measurements. Furthermore, even though the separation of the two $3p$ channels is only 0.1 eV, the RABBITT side-bands can be tuned very accurately to span much narrower features of the photoelectron spectrum like Fano resonances [14, 23]. And, the newly-implemented spin-polarization spectroscopy [19] could also be used to separate the two channels. But even if the two $2p$ channels are not separated, interesting phenomenology in the time delay remains, as indicated in Fig. 4.

IV. CONCLUSION

In conclusion, using the photodetachment of Cl^- as a case study, the calculations demonstrate that Wigner time delays of outer-shell photoemission in the vicinity of inner-shell thresholds for negative ions are dominated by many-body correlations in the form of interchannel coupling which give rise to time delays that are quite large and exhibit a very complex energy dependence, much different from the situation for neutral atom photoemission. In addition, relativistic interactions are extremely important, an unexpected result at such low Z. Finally, the

results suggest a fruitful area for experimental inquiry. With a recent expansion of attosecond spectroscopy to a broader photon energy range [16, 36], experimental verification of the present results is becoming within the reach.

V. ACKNOWLEDGEMENTS

This work is enabled by the infrastructure and support extended to our research group by the Director, Indian Institute of Technology Tirupati, which includes hospitality to SS and STM. This work was supported by the Chemical Sciences, Geosciences, and Biosciences Division, Office of Basic Energy Sciences, Office of Science, US Department of Energy.

[1] E. P. Wigner, Phys. Rev. **98**, 145 (1955).
[2] L. E. Eisenbud, Ph. D. thesis, Princeton Univ. (1948).
[3] F. T. Smith, Phys. Rev. **118**, 349 (1960).
[4] M. Schultze *et al*, Science **328**, 1658 (2010).
[5] K. Klünder *et al*, Phys. Rev. Lett. **106**, 143002 (2011).
[6] R. Pazourek *et al*, Rev. Mod. Phys. **87**, 765 (2015) and references therein.
[7] T. Barillot *et al*, Phys. Rev. A **91**, 033413 (2015).
[8] A. S. Kheifets *et al*, Phys. Rev. A **92**, 063422 (2015).
[9] M. Sabbar *et al*, Phys. Rev. Lett. **115**, 133001 (2015).
[10] P. Hockett *et al*, J. Phys. B **49**, 095602 (2016).
[11] M. Huppert *et al*, Phys. Rev. Lett. **117**, 093001 (2016).
[12] S. Heuser *et al*, Phys. Rev. A **94**, 063409 (2016).
[13] V. Gruson *et al*, Science **354**, 734 (2016).
[14] M. Kotur *et al*, Nat. Comm. **7**, 10566 (2016).
[15] A. S. Kheifets *et al*, Phys. Rev. A **94**, 013423 (2016).
[16] M. Isinger *et al*, Science **358**, 893 (2017).
[17] D. A. Keating *et al*, J. Phys. B **50**, 175001 (2017).
[18] L. Gallmann *et al*, Struct. Dynam. **4**, 061502 (2017).
[19] M. Fanciulli *et al*, Phys. Rev. Lett. **118**, 067402 (2017).
[20] C. A Nicolaides, Appl. Sci. **8**, 533 (2018).
[21] D. A. Keating *et al* Phys, Rev. A **98**, 013420 (2018).
[22] P. C. Deshmukh *et al*, J. Phys. B **51**, 065008 (2018).
[23] C. Cirelli *et al*, Nat. Comm. **9**, 955 (2018).
[24] J. Vos *et al*, Science **360**, 1326 (2018).
[25] W. Drube *et al*, J. Phys. B **46**, 245006 (2013).
[26] S.J. Buckman and C.W. Clark, Rev. Mod. Phys. **66**, 539 (1994) and references therein.
[27] E. Lindroth and J. M. Dahlström, Phys. Rev. A **96**, 013420 (2017).
[28] A. S. Kheifets *et al*, Phys. Rev. Lett. **117**, 143202 (2016).
[29] J. M. Dahlström *et al*, J. Phys. B **45**, 183001 (2012).
[30] W. R. Johnson and C. D. Lin, Phys. Rev. A **20**, 964 (1979).
[31] J. Wätzel *et al*, J. Phys. B **48**, 025602 (2015).
[32] A. Mandal *et al*, Phys. Rev. A **96**, 053407 (2017).
[33] J. Jose *et al*, Phys. Rev. A **80**, 023405 (2009) and references therein.
[34] E. W. B. Dias *et al*, Phys. Rev. Lett. **78**, 4553 (1997).
[35] S. Saha *et al*, Phys. Rev. A **99**, 043407 (2019).
[36] A. Jain *et al*, Optics Lett. **48**, 4510 (2018).